FERMI
national accelerator laboratory

TM-582
0710.000

Feasibility Study of a Gas Jet Target Without Liquid Helium for Use in the Main Ring

P. Mantsch and F. Turkot

June 6, 1975

Summary

A study has been carried out on the feasibility of a gas jet target for use in the main ring. This target would operate at room temperature, as contrasted with the target presently in use which requires liquid He. As part of this effort, a prototype target was assembled using a 0.004" de Laval nozzle and oil diffusion pumps; measurements were made on target densities, jet profiles, and differential pumping schemes with H_2 gas. We conclude that a competitive target can be made and would have major advantages in reliability and cost of operation.

1. Introduction

1.1 Physics Utility of a Gas Jet Target in the Main Ring

The value of using a gas jet target in the main ring during acceleration to do particle physics experiments is by now well established;[1] some of the unique advantages this technique affords are:

a) a continuous broad range of incident energy (8 - 400 GeV) available during a repetitive 3-sec period, with good definition at any one energy,

b) an ultra-thin target ($\sim 10^{-7}$ g/cm^2) which allows precision measurements on low energy products,

c) a well defined incident beam with $<<$ 1% halo,

d) a high interaction rate, $\sim 2.4 \times 10^9$/sec for 2×10^{13} protons/pulse on a H_2 jet target with $\rho\ell = 1 \times 10^{-7}$ g/cm^2, which is equivalent to a beam of 5×10^{10} p/sec on a 1' long liquid hydrogen target or an instantaneous luminosity of 6×10^{34} cm^{-2} sec^{-1}.

1.2 Current Jet Target Technology

A gas jet target, built in the U.S.S.R.[2] by the Dubna Laboratory, has been in use in the Internal Target Area at C0 since July of 1972; it has been used in a series of successful investigations to study pp and pd interactions. This target utilizes liquid He both to cool the gas injected into the vacuum chamber and to cryopump the gas after it has passed through the beam. The use of liquid He necessarily entails a certain degree of technical sophistication, complexity, and operating expense; it also imposes some constraints which may be a limitation for certain types of experiments using a gas jet target. While

cryopumping at 4.2°K is a very effective pump for H_2 and D_2, it is not nearly as useful for He, which is also a target of interest.[3] Finally, there has been considerable difficulty in keeping the present jet operational during the past eight months. Under these circumstances, we thought it might be useful to examine possible alternatives to a liquid He type jet target.

1.3 Scope of this Study

We are aware of three efforts[4] to make jet targets without liquid He, all three have produced operating jets. The problem of an alternative to a liquid He (LHe) jet target is therefore not one of demonstrating existence, but rather to make (or to know how to make) an operational target that matches the particular constraints imposed by operating at C0 and that competes favorably with the present LHe jet.

In this report we first review some of the basic facts concerning the use of jet targets. We then discuss the operating characteristics of and experience with the LHe target. This is followed by a simple quantitative model of jet target operation. Next we describe some test bench work on a room temperature (RT) jet using a de Laval nozzle of 0.004" throat diameter. The objectives there were to: (a) demonstrate a good jet profile, (b) determine the range of densities attainable, and (c) test out a differential pumping scheme. Finally we make a comparison between a possible RT jet and the present one.

2. Target Requirements and Constraints

2.1 Desirable Target Features from the Experimental Side

Past experience and future plans indicate that the following features are desirable in a gas jet target.

1. A variable range of target thickness ($\rho \ell$) from 1×10^{-8} - 5×10^{-7} g/cm^2 (see Sec. 2.2 below).

2. A reasonable target-on time during the 3-sec acceleration period, i.e., ≥ 10% or 300 msec.

3. Continuous operation with good reliability and low overhead.

4. Transverse dimension of the jet approximately equal to the horizontal size of the beam, the beam has FWHM = 1.5 cm at 10 GeV and ~ 2 mm at 300 GeV, changing as $1/\sqrt{P}$.

5. A density of gas not in the jet proper (ρ_{BKG}) << ρ_{JET}, e.g., $\rho_{BKG} \leq \rho_{JET}/1000$.

6. As little as possible material close to the interaction region, e.g., in a 12-cm diameter cylinder centered on the beam.

7. Good access to the interaction region for detectors and monitors.

8. Ability to run with a variety of gases in addition to H_2, D_2, and He.

9. Simple design, such that an operational spare is available and can be installed in ~ 1 hour.

2.2 Constraints Imposed by Main-Ring Operation

1. Dependable access only once per week for ~ 8-hour period.

2. Limits on type and amount of gas injected into main-ring vacuum system outside of C0, particularly He.

3. Small attenuation (< .1%) of the accelerated beam.

4. No affect on extraction efficiency of beam from main ring. Recent tests at C0 indicate that a localized, pulsed, H_2 gas burst of $\rho\ell = 5 \times 10^{-7}$ g/cm^2 lasting ~ 0.5 sec could have detrimental effects on extraction at beam intensities of 2×10^{13} per pulse.[5]

3. Operating Characteristics of and Experience with the Dubna Jet Target

The present Dubna jet geometry is shown in Fig. 1. It works as follows: cooled H_2 or D_2 gas ($\sim 30^{\circ}K$) at $\approx$ 1 atm pressure is injected in a pulsed mode through a nozzle of diameter 0.3 mm (.012"); about 97% of the gas is trapped instantaneously in the cup and on the top surface of the cryopump, the remaining 3% is pumped with a time constant of $\sim$0.1 sec (corresponding to a pumping speed of $\sim$ 3000 ℓ/s) mainly by the top surface of the cryopump, a copper surface of $\sim$ 400 cm^2 at 4.2°K. Each pulse is $\sim$ 35 cm^3 of STP H_2 gas; after $\sim$ 3 hours of operation at 3 pulses/cycle and 500 cycles/hr, about 160 ℓ of STP H_2 has been trapped (equivalent to 14 g or $(5.4\ cm)^3$ of solid H_2) "filling" the cup of the cryopump. The main-ring beam is interrupted, the entire assembly is then raised, sealed off from the main-ring vacuum, the LHe is purged and the solid H_2 sublimated. Typical operating ranges and conditions[1] are:

Width of jet (FWHM) at 15 mm from nozzle	12 mm
Width of jet (FWHM) at 25 mm from nozzle	24 mm
Opening angle of jet	$\sim 40^{\circ}$
Temperature of gas before nozzle, T_o,	20-40°K
Pressure of gas before nozzle, P_o,	0.5 - 4 atm
Density of jet at 15 mm	0.4 - 3 x 10^{-7} g/cm^3
Duration of gas pulse	250 ms
Number of pulses per 3 sec of acceleration	3

Sideview of Dubna liquid helium gas jet target.

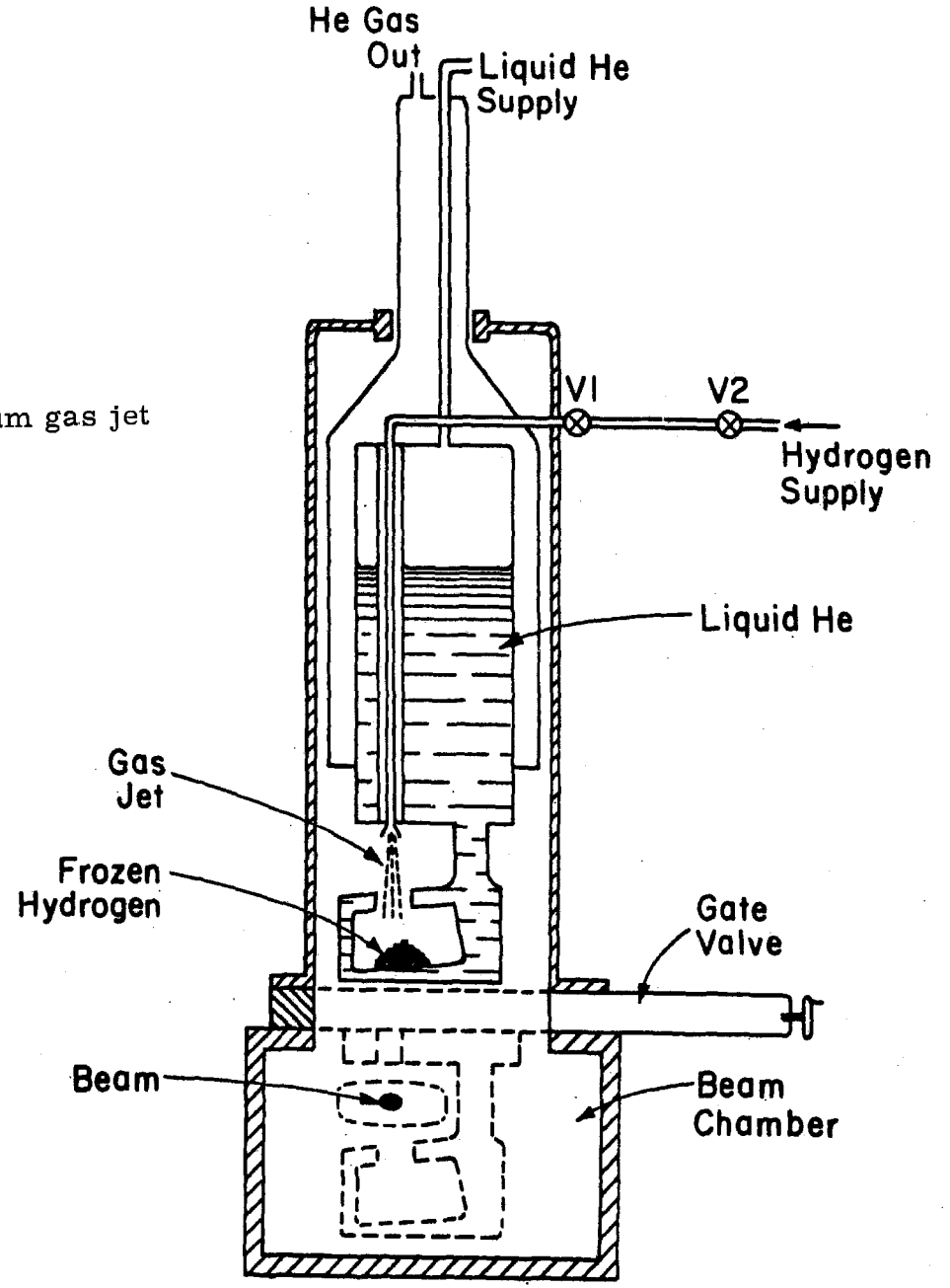

Fig. 1

Sublimation period	40 min
Continuous operating period	2-4 hrs
LHe consumption	20 - 40 ℓ/hr

Each jet pulse is accompanied by a pressure transient in the surrounding vacuum chamber. For a pulse of time duration t_o into a chamber of volume V, this transient has the form (see Sec. 4.2).

$$P(t)-P_{BASE} = \frac{Q(T_o, P_o)}{S} \quad (1-\epsilon_{CRYO}) \quad (1-e^{-t/\tau}), \; 0< t\leq t_o \tag{1}$$

$$= (P(t_o)-P_{BASE})e^{-t/\tau}, \quad t>t_o \tag{2}$$

where

$Q = P\frac{dv}{dt}$ = the flow rate of gas through the nozzle

ϵ_{CRYO} = the efficiency of the cryopump for instantaneous trapping, ~ 97%

S = the effective pumping speed for non-trapped gas, ~ 3000 ℓ/s

τ = V/S, ~ 100 msec

P_{BASE} = base pressure at $t< 0$

(these numbers are consistent with the data of Golovanov, et al[6])

So for $T_o = 20^oK$ and P_o in atm one gets

$$P(t) - P_{BASE} = 1.6 \times 10^{-3} \; P_o \; (1-e^{-t/\tau}) \text{ Torr} \tag{3}$$

which implies pressure peaks of 1.6 microns at a P_o of 1 atm. The density of the jet will also be proportional to P_o; at 15 mm from the nozzle, the ratio of target density to background density[7] is ~ 400.

The LHe for the target is supplied by a C.T.I.-1400 liquifier, having a capacity of 30-35 ℓ/hr. Although the static boil-off rate of the target proper has been as low as 9 ℓ/hr, it is variable and in the past, sufficient LHe to support continuous operation of the target for the 6-day period between scheduled accelerator down periods has not been achieved; a 50% duty cycle is typical.

After a two-year period of use, the present target was plagued by a series of cold leaks from the LHe vessel into the vacuum chamber; such leaks are often difficult to locate. On one occasion ≈ 20 ℓ(STP) of He gas leaked into the vacuum chamber, resulting in an impairment of the leak-hunting ability in the main ring due to He contamination of the ion pumps.

4. Model of Jet Target Operation

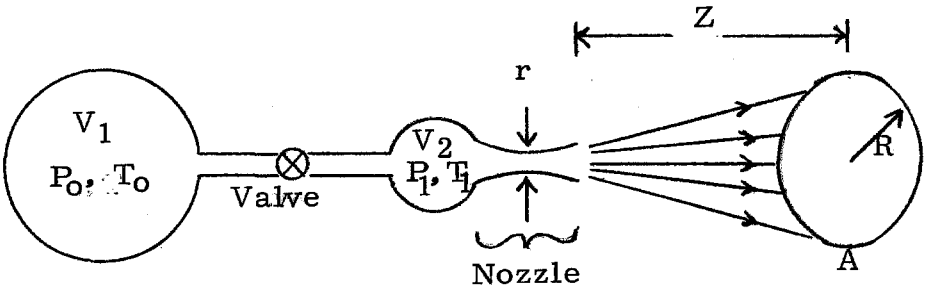

Fig. 2

In practice, a gas jet is formed (see Fig. 2) by quickly (~ 5 msec) opening a solenoid valve which allows the gas, which is under some starting values (P_o, T_o), to flow into an evacuated volume V_2 which is connected to high vacuum (~ 10^{-6}t) through

a de Laval nozzle.[9] The nozzle has a constriction of the order 0.2 mm, V_2 is the unavoidable volume (usually ~ 3 cm^3) between the valve and the nozzle. The gas in V_2 has $P_1 \simeq P_o$ $T_1 \simeq T_o$ (unless cooled as in Dubna jet), it then expands through the nozzle into the vacuum, developing a stationary conical shaped jet after a few msecs. The flow velocity of the gas in the jet is supersonic and approximately equal to the speed of sound in V_2, e.g., if $T_1 = 295^oK$ about 1.8 m/msec for H_2.

4.1 Model Relating Density, Profile, and Flow

An exact description of the steady-state profile (e.g., density and velocity distribution at each point in the vacuum chamber) is impossible to calculate theoretically. However, a useful description (which does not predict, but rather uses the profile as a parameter) can be obtained by taking a one-dimensional gas-dynamics flow model[10] that assumes an ideal gas in a steady-state, isentropic flow (so called "strong form" of Bernoullis law). The basic parameters are obviously P_o, T_o, and r (radius at narrowest point of nozzle), if we take as a fourth parameter R, the radius of the jet where it intersects the beam, then we can easily derive an expression for the gas density, ρ, at the beam position

$$\rho = \left(\frac{r}{R}\right)^2 \frac{P_o M}{C T_o} \left(\frac{2}{\gamma + 1}\right)^{\frac{1}{\gamma - 1}} \left(\frac{\gamma - 1}{\gamma + 1}\right)^{1/2} \qquad (4)$$

where:

M = molecular weight

γ = ratio of specific heats

C = molar gas constant

For $\gamma = \frac{7}{5}$, M = 2.016, this becomes

$$\rho = 215.5 \left(\frac{r}{R}\right)^2 P_o(\text{atm}) \frac{295}{T_o} \times 10^{-7} \frac{g}{cm^3} \tag{5}$$

A quantity of practical interest is the gas flow, $Q = P\frac{dv}{dt}$, measured at some temperature T_i,

$$Q = \pi r^2 P_o \left(\frac{2}{\gamma + 1}\right)^{\frac{1}{\gamma - 1}} \left(\frac{2\gamma}{\gamma + 1}\right)^{1/2} \left(\frac{C}{MT_o}\right)^{1/2} T_i \tag{6}$$

or evaluating as above for $T_i = 295^oK$ (r in cm)

$$Q = \pi r^2 \times 755 \times 10^2 \times P_o(\text{atm}) \times \sqrt{\frac{295}{T_o}} \quad \frac{\text{atm-cm}^3}{\text{sec}} \tag{7}$$

Using eqs. (4) and (6) one can relate Q and ρ as follows

$$Q = \pi R^2 \rho \sqrt{\frac{\gamma}{\gamma - 1}} \sqrt{\frac{2CT_o}{M}} \quad \frac{C T_i}{M} \tag{8}$$

which at $T_i = 295^oK$ evaluates to

$$Q = 350.5 \times \pi R^2 \rho \, (10^{-7} \text{ g/cm}^3) \sqrt{\frac{T_o}{295}} \quad \frac{\text{atm-cm}^3}{\text{sec}} \tag{9}$$

From (8) we note that

$$Q \propto \rho \sqrt{T_o} , \tag{10}$$

i.e., for fixed ρ, Q goes as $\sqrt{T_o}$; and that for fixed Q, ρ goes as $(T_o)^{-1/2}$. If we do not fix ρ or Q but simply vary T_o then from (4) and (6) we see

$$\rho \propto \frac{1}{T_o} \text{ and } Q \propto \frac{1}{\sqrt{T_o}} . \tag{11}$$

From (8) we can also define a "figure of merit" for given nozzle as ρ/Q, giving

$$F \equiv \rho/Q \propto \frac{1}{R^2\sqrt{T_o}} \tag{12}$$

If $\rho\ell$ is the quantity of interest then the merit figure would be

$$F' \equiv \frac{R\rho}{Q} \propto \frac{1}{R\sqrt{T_o}} \tag{13}$$

Experimentally one finds that the shape of the jet for a given nozzle is independent of P_o once it is above a certain value. Data on the dependence with T_o is less complete, but it appears to be weakly dependent also.[12]

4.2 Model of the Vacuum System

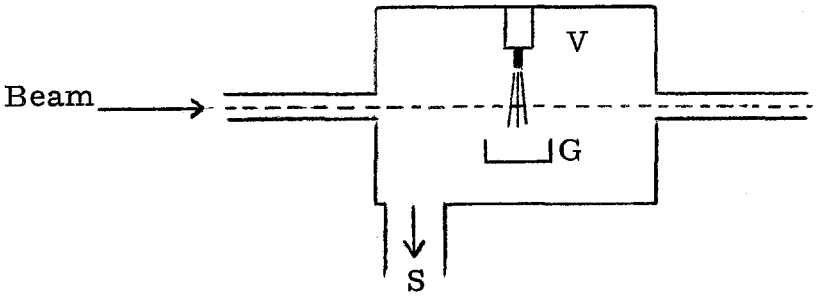

Fig. 3

One can approximate the vacuum system as shown in Fig. 3. The jet mechanism is contained in a "target box" of volume V; G is a device which instantaneously captures a fraction ϵ of the directed gas issuing from the nozzle, while S is a pump that pumps via molecular flow (at a temperature T_i) the fraction of gas, $1 - \epsilon$, not captured by G. In the Dubna jet G is the cavity of the cryopump and S the top surface of the

cryopump; in a warm jet G would be a differential pumping aperture and S a conventional vacuum pump. The pressure transient that accompanies the pulsing of the jet for a period t_o is given by

$$P(t) - P_{BASE} = \frac{Q(r, T_o, P_o)}{S} (1-\epsilon)(1-e^{-t/\tau}), \quad 0<t\leq t_o \tag{14}$$

$$= (P(t_o)-P_{BASE})e^{-t/\tau}, \quad t>t_o$$

where $\tau = V/S$. The peak of the pressure transient, P_M, occurs at $t = t_o$, with $P_M \leqq \frac{Q(1-\epsilon)}{S}$. The undesirable interactions arising from the background gas outside of the jet vary like P_M, hence one measure of the target's usefulness is the ratio ρ/P_M

$$\frac{\rho}{P_M} = \frac{\rho S}{Q(1-\epsilon)(1-e^{t_o/\tau})} \tag{15}$$

$$= F \frac{S}{(1-\epsilon)(1-e^{t_o/\tau})}$$

where F is the nozzle figure of merit as defined in eq. (12) and the other factors depend on the pumping scheme. Instead of P_M, it is better to use the peak density, ρ_M, giving

$$\rho/\rho_M = F \frac{S}{(1-\epsilon)(1-e^{-t_o/\tau})} \frac{C T_i}{M}$$

$$= \frac{S}{(1-\epsilon)(1-e^{-t_o/\tau})} \frac{1}{\pi R^2} \sqrt{\frac{\gamma-1}{\gamma}} \sqrt{\frac{M}{2C T_o}} \tag{16}$$

Evaluating this for H_2 yields

$$\rho/\rho_M = \frac{S(\ell/sec)}{(1-\epsilon)(1-e^{-t_o/\tau})} \; 1.09 \times 10^{-3} \sqrt{\frac{295}{T_o}} \; \frac{1}{R^2_{(cm)}} \qquad (17)$$

5 Jet Apparatus with Los Alamos Nozzle

5.1 The Nozzle Assembly

A continuous duty gas jet target was recently developed by Brolley[4] for use at the LAMPF machine at Los Alamos. In the course of this work, techniques were devised for making de Laval type converging-diverging nozzles of very small throat diameter (.002 to .010 cm). The nozzle used in the present studies was provided by Brolley. A sketch of this nozzle and its dimensions are shown below:

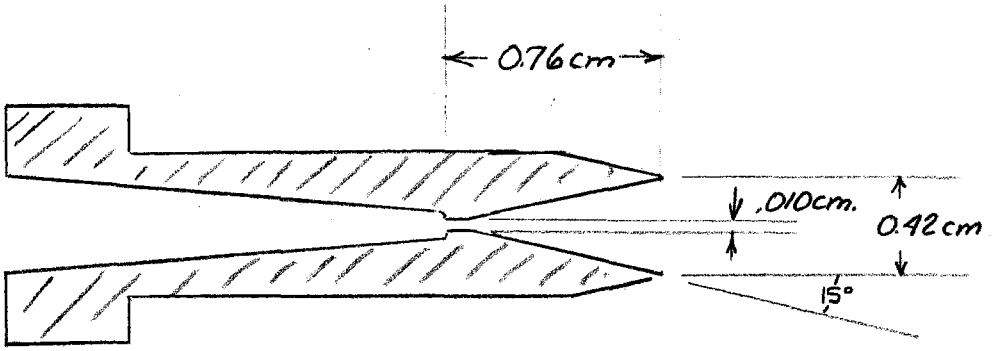

THE LOS ALAMOS NOZZLE

Fig. 4

The test setup is sketched in Fig. 5. The nozzle was mounted on the end of a tube that extended through the top plate of the test chamber. A sliding vacuum seal allowed the nozzle assembly to move vertically within the test chamber about 24 cm.

FIGURE 5

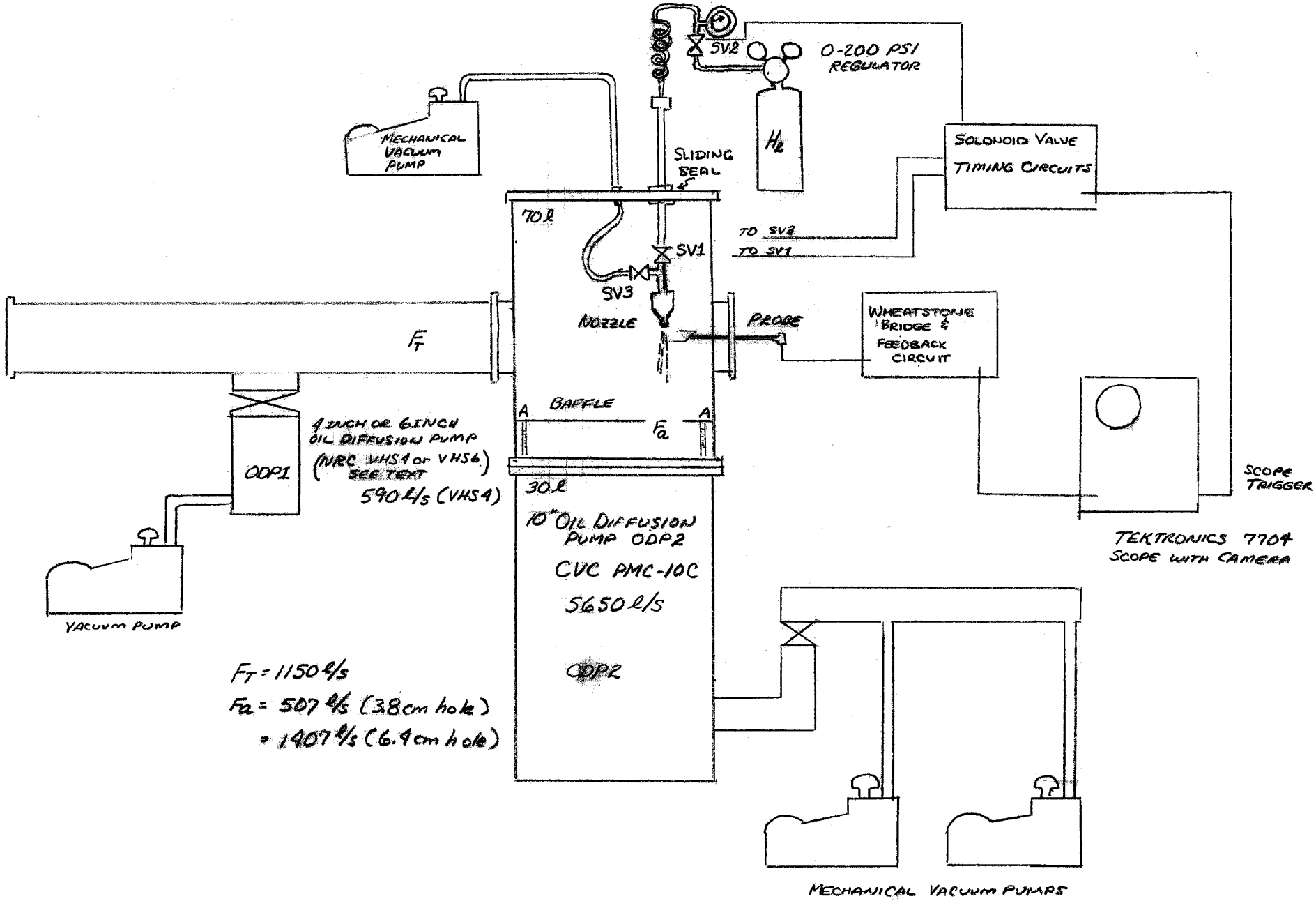
SV2
0-200 PSI REGULATOR
MECHANICAL VACUUM PUMP
SLIDING SEAL
H_2
SOLENOID VALVE
TIMING CIRCUITS
TO ℓ
TO SV2
TO SV1
SV1
SV3
NOZZLE
PROBE
WHEATSTONE BRIDGE & FEEDBACK CIRCUIT
F_T
A
BAFFLE
A
F_a
4 INCH OR 6 INCH OIL DIFFUSION PUMP (NRC VHS4 or VHS6) SEE TEXT
590 ℓ/s (VHS4)
ODP1
30 ℓ
10" OIL DIFFUSION PUMP ODP2
CVC PMC-10C
5650 ℓ/s
ODP2
SCOPE TRIGGER
TEKTRONICS 7704 SCOPE WITH CAMERA
VACUUM PUMP
F_T = 1150 ℓ/s
F_a = 507 ℓ/s (3.8cm hole)
= 1407 ℓ/s (6.4cm hole)
MECHANICAL VACUUM PUMPS

5.2 The Gas Pulsing System

The target gas was fed from a hydrogen gas bottle via a 0-200 PSI regulator to a buffer volume above the nozzle assembly. The solenoid valve,SV1,admitted gas from the buffer volume to the nozzle. Another solenoid valve,SV2,controlled the flow of the gas from the bottle to the buffer volume.

Because of the small size of the nozzle orifice, the charge of gas admitted by SV1 to the nozzle escaped very slowly. This resulted in a long "tail" on the jet pulse. In order to make a sharp cutoff on the pulse length , a mechanical vacuum pump was connected through a third solenoid valve, SV3, to the volume just before the nozzle.

The operation of these valves was sequenced by means of the timing circuit shown in Fig. 6. The start trigger opened valve SV1 to initiate the jet pulse. After a delay, approximately equal to the desired pulse width, valve SV3 was opened long enough to stop gas flow through the nozzle and to remove residual gas. Valve SV2 was opened when SV3 was closed to recharge the buffer volume.

5.3 The Test Chamber and Vacuum System

The test chamber containing the nozzle assembly was mounted directly to the flange of a 10-inch oil diffusion pump (CVC model PMC-10). The nozzle assembly was offset with respect to the center of the diffusion pump so that the H_2 gas jet was directed into the oil vapor jet.

Another oil diffusion pump (NRC model VHS -6) with valve and water-cooled baffle was connected to the test chamber through a length of 6-inch beam pipe.

FIGURE 6

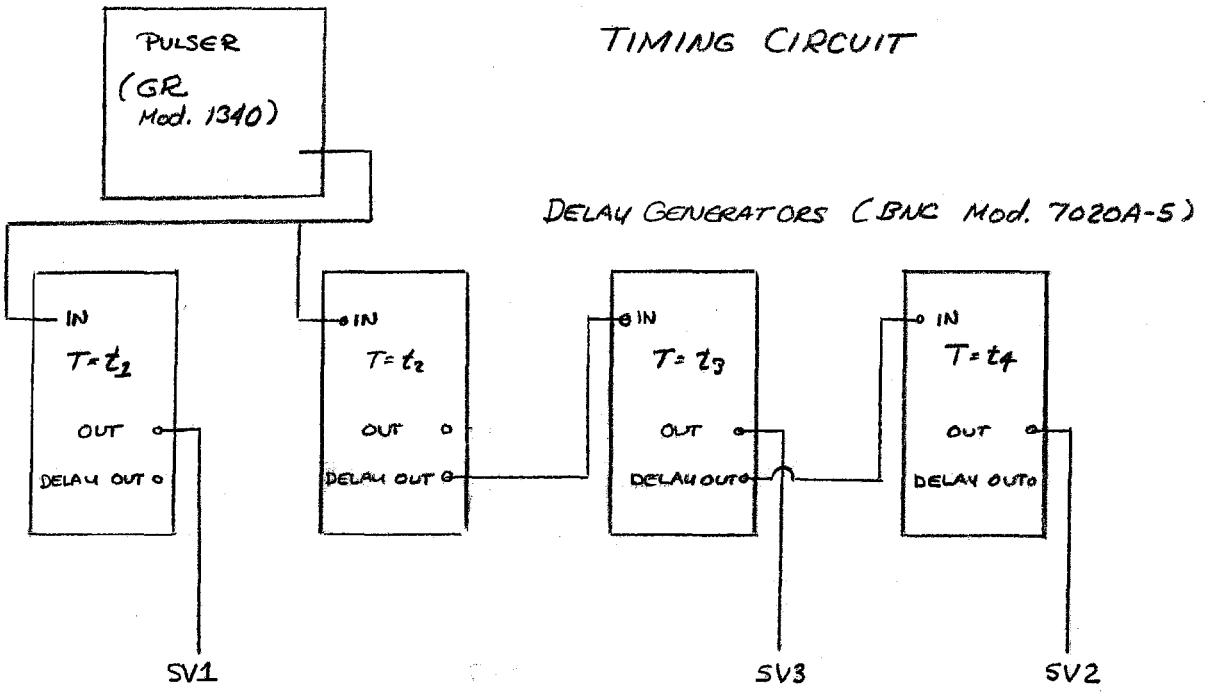
TIMING CIRCUIT
PULSER
(GR
Mod. 1340)
DELAY GENERATORS (BNC Mod. 7020A-5)
IN
T = t1
OUT
DELAY OUT
IN
T = t2
OUT
DELAY OUT
IN
T = t3
OUT
DELAY OUT
IN
T = t4
OUT
DELAY OUT
SV1
SV3
SV2

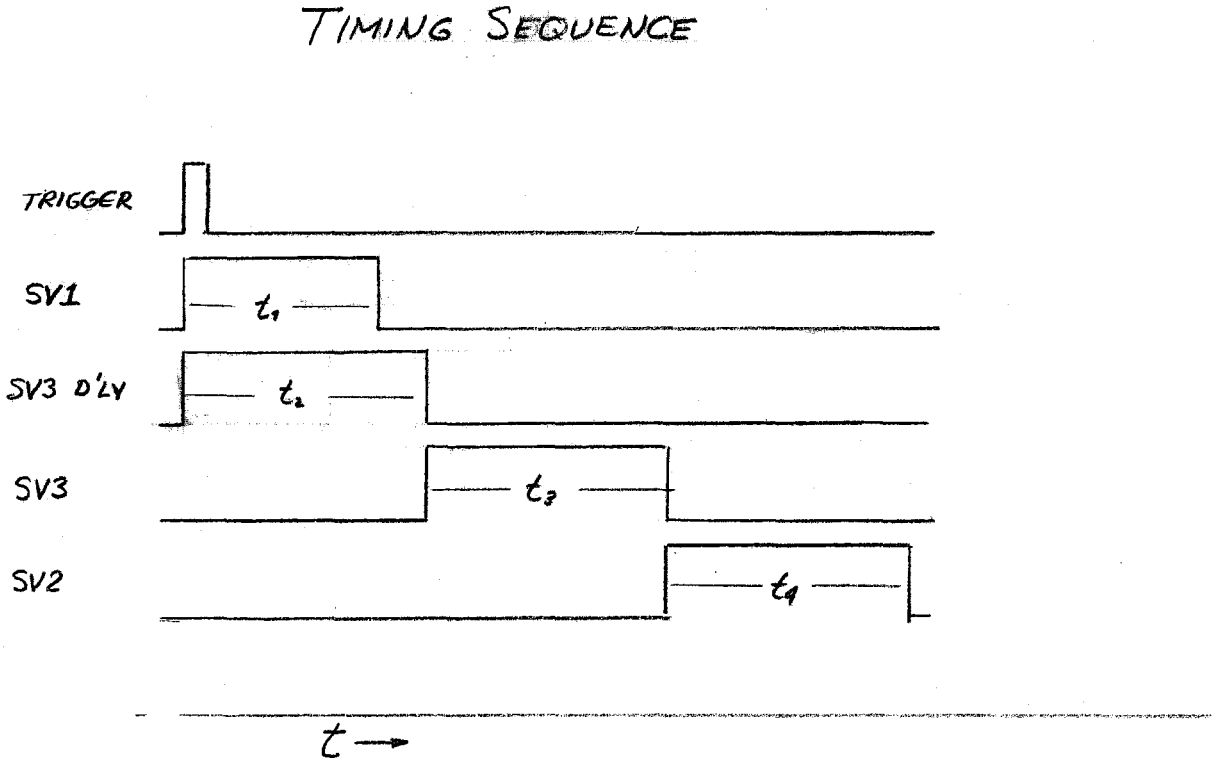
TIMING SEQUENCE
TRIGGER
SV1
t1
SV3 D'LY
t2
SV3
t3
SV2
t4
t →

A differential pumping scheme was effected by mounting a removable 1/16" thick aluminum baffle over the top flange of the 10-inch pump. A hole in the baffle plate (either 3.8 cm or 6.4 cm diameter) was oriented directly below the jet nozzle. The nozzle could be moved vertically with respect to the hole to measure the effective trapping of the jet gas below the baffle. Any gas not trapped by the baffle and 10-inch pump was pumped away by the 6-inch D.P.

The pressure in the vacuum system was measured by a thermocouple gauge and an ion gauge.

5.4 Apparatus for Profile Measurement

A constant current anemometer (CTA) was used to investigate the properties of the Los Alamos nozzle. The detailed operation of the CTA of the type used in these studies is described in Ref. 4(a).

The circuitry for the anemometer is shown in Fig. 7. The probe consists of a 5-micron platinum-coated tungsten wire which forms one leg of a wheatstone bridge. The bridge is balanced with current in the probe wire sufficient to maintain a temperature of about 900°K. The jet gas moving past the wire removed energy from the wire by molecular collisions thus trying to cool the wire and reduce its resistance. A differential amplifier across the bridge sensed the imbalance causing a feedback signal to be generated which increased the voltage at the top of the bridge to restore the balance. A scope, triggered by the gas jet pulse, recorded the time variation ΔV on the bridge. The density of particles hitting the anemometer wire is proportional to the power variation ΔW in the wire. The relationship

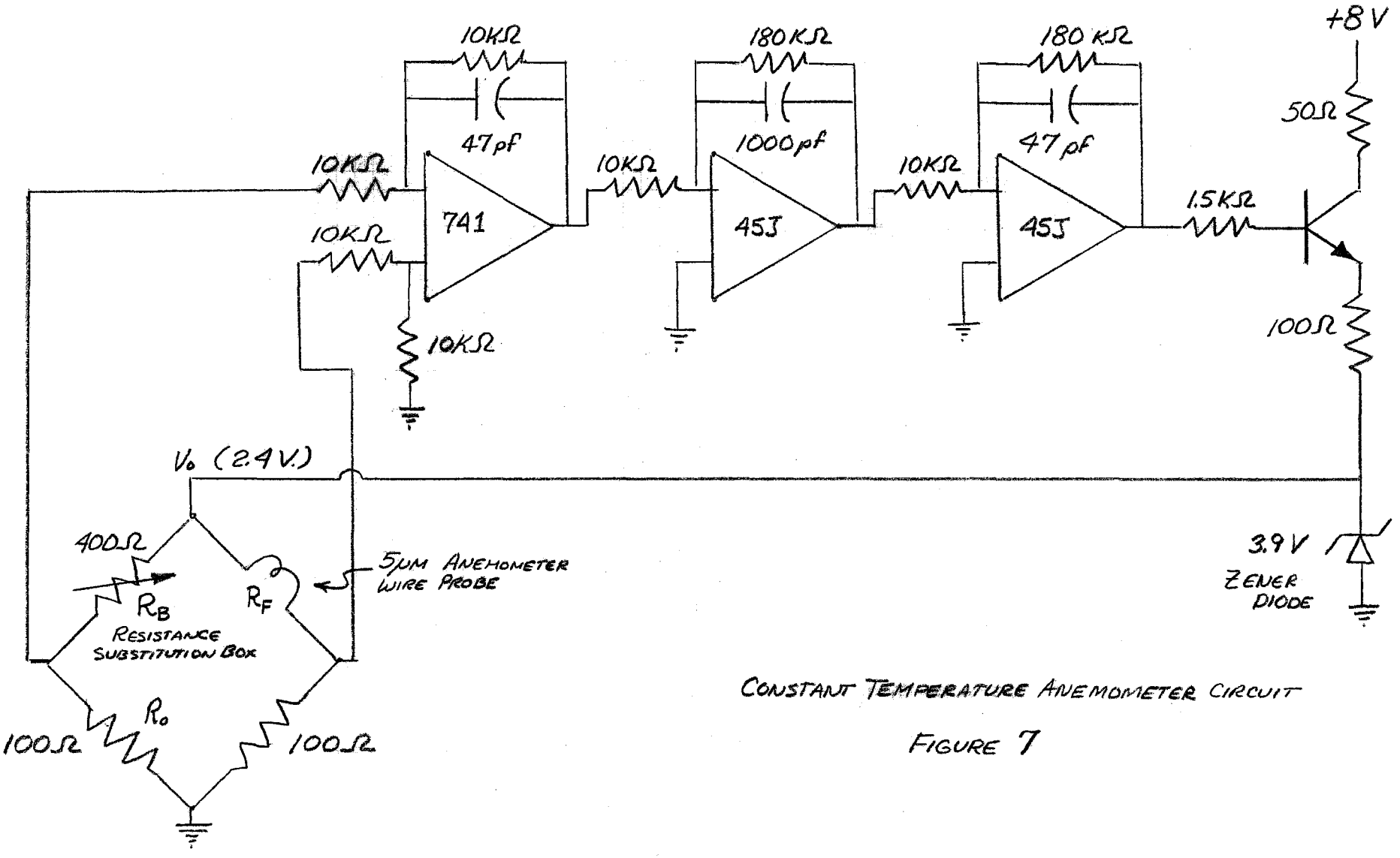

CONSTANT TEMPERATURE ANEMOMETER CIRCUIT

FIGURE 7

between ΔW and ΔV is given by

$$\frac{\Delta W}{W_o} = 2\frac{\Delta V}{V_o}\left(1 + \frac{\Delta V}{2V_o}\right) \tag{18}$$

$$W_o = \frac{V_o^2 R_F}{(R_F + R_o)^2}$$

where R_o and R_F are the resistance values of the legs of the bridge as shown in Fig. 6 and V_o is the quiescent voltage at the top of the bridge. The scope traces of ΔV were recorded with a polaroid scope camera.

The probe containing the anemometer wire was mounted in a sliding vacuum seal in a port window of the test chamber. To measure jet density profiles, the probe was moved horizontally past the jet. To measure profiles in different horizontal planes, the jet nozzle was moved vertically.

6. Measurements and Calibration with RT Jet Apparatus

6.1 Measurements

The investigation proceeded in two parts. First, the flow characteristics of the Los Alamos (LA) nozzle were examined and operating conditions were varied to achieve a gas jet with a good profile and reasonable density range. The second part of the study focused on the problem of pumping the jet gas. An effort was made to realize a pumping configuration compatible with experimental requirements and operating restrictions particular to the Internal Target Area.

Jet profile measurements were made to determine the shape dependence on gas pressure. Since the probe also measured gas density, the behavior of the density with pressure was studied for comparison with a model of gas flow. Detailed profile measurements were made at gas pressures before the nozzle of 35, 95 and 135 PSIA. The upper limit of the pressure was restricted by the capacity of the vacuum system.

Profiles were made by moving the probe transverse to the jet in increments of 0.8 mm. Profiles were made in planes at several vertical distances from the nozzle. The range of displacements from the nozzle (9 to 44 mm) was typical of those one would encounter in an actual target in the main ring where the nozzle position was fixed with respect to the beam.

Once the jet shape was measured and a reasonable operating density was selected, the response of the vacuum system was studied. Pumping speed of the large 10-inch diffusion pump was measured with various nozzle positons to see if the speed was enhanced if the jet was directed into the oil stream of the pump. Studies were made with a baffle over the mouth of the 10-inch D.P. A hole in the baffle directly below the nozzle was sized to be slightly larger than the cone of the jet. Two hole sizes were used; 3.8 cm and 6.4 cm. Measurements were made of the quantity of gas from the jet that was "trapped" by the large pump. The recovery times of the vacuum system were measured under all conditions for comparison with calculation and so that a system optimum for an actual target could be projected.

6.2 Calibration of Vacuum Gauges and CTA

Absolute dc calibration of the three gauges used (thermocouple, ion gauge[11] (Bayard-Alpert), and CTA) in the 1-200 micron range for H_2 was accomplished by injecting a known quantity of H_2 gas into the main chamber of Fig. 5 with all pumps closed off. The leak-up rate of the main chamber after ~ 24 hrs of pumping was ~ 2×10^{-5} t/min as read on the I.G. (air calibration). The known quantity of H_2 gas was obtained by opening only SV1 (see Fig. 5) for ~ 25 msec; the pressure in the known volume (56 cm^3) between SV1 and SV2 was recorded before and after the opening. The nozzle discharges the volume between SV1 and the nozzle rather slowly (1/e in 640 msec for a 4-CM^3 volume). Hence a 4-cm^3 pulse at 17.5 PSIA into the 115 ℓ volume gives a pressure rise of

$$\Delta P = 4.0 \times \frac{17.5}{14.7} \times \frac{1}{115 \times 10^3} \times 760 = 31.5 \times 10^{-3} t.$$

This cycle was repeated five times yielding a curve with equal steps in pressure from 31-158 $\times 10^{-3}$ t. The range from 2-13 $\times 10^{-3}$t was covered in 7 pulses by opening SV1 and then terminating after ~ 20 msec by opening SV3. The CTA incremental power (ΔW) was observed to be linear with pulse number and to extrapolate through zero ($P_{BASE} = 10^{-6}$t) in both ranges, hence it was used to establish the absolute calibration of the low range.

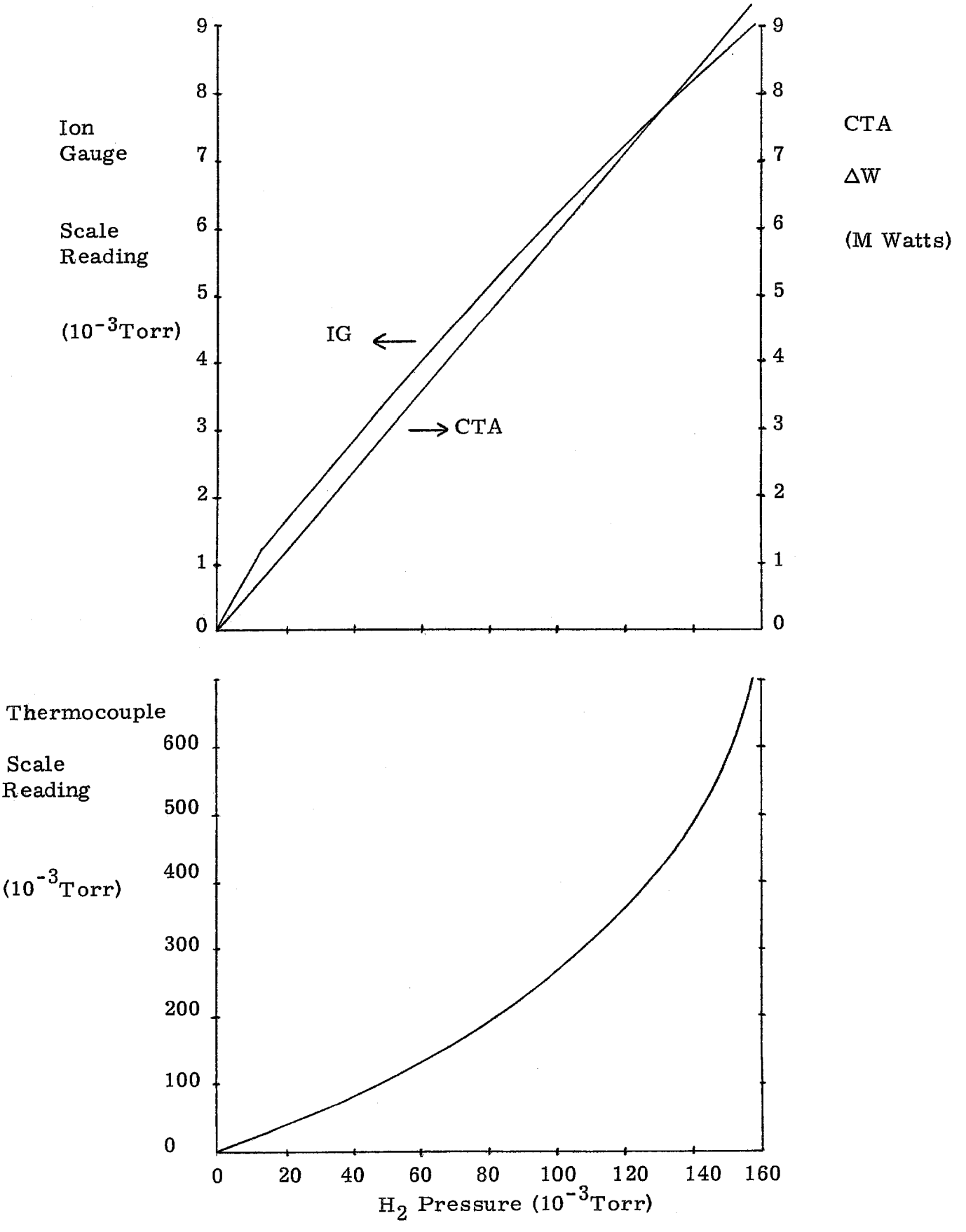
Ion Gauge Scale Reading (10^{-3}Torr)
CTA ΔW (M Watts)
IG
CTA
0
1
2
3
4
5
6
7
8
9
Thermocouple Scale Reading (10^{-3}Torr)
0
100
200
300
400
500
600
0
20
40
60
80
100
120
140
160
H_2 Pressure (10^{-3}Torr)

Fig. 8

The result of the H_2 calibration is shown in Fig. 8 for all three gauges. We note that:

a) Thermocouple gauge - in the range of scale reading (air calibration) from 4-140 x 10^{-3}t it reads too high a H_2 pressure by a factor ~ 2.2, above this range it diverges, being too high by 4.4 at a scale reading of 700 x 10^{-3} t.

b) Ion gauge - in the scale range (air calibration) 1.5-13 x 10^{-4}t it reads too low a H_2 pressure by a factor of 10, a kink occurs at a scale reading of 1.3 x 10^{-3}t after which it becomes progressively less sensitive, being a factor of 20 low at a scale reading of 9 x 10^{-3}t.

c) CTA - it appears quite linear over the range of H_2 pressure from 1.8 - 160 x 10^{-3} with a sensitivity, $\frac{dW}{dP}$, of 0.06 mW/10^{-3}t, corresponding to a voltage signal of ~ 0.8 mV/10^{-4}t. Normal operating conditions were R = 400 Ω, corresponding to a power dissipation, W_o, of 8.8 mW and a temperature of 900°K.

Under high localized gas pulses, we observed an unusual time dependence of the CTA signal (drops by factor of 2 after ~ 10 msec), this occurs at high pressure (≥ 80 PSIG) when the CTA is within 4 mm of the nozzle where the FWHM of the jet is ~ 3 mm. Under these conditions the power absorbed by the gas, ΔW, is ≈ W_o, which presumably results in a substantial range in the temperature distribution along the CTA wire. The dc calibration of Fig. 8 is estimated to be accurate to ± 20%.

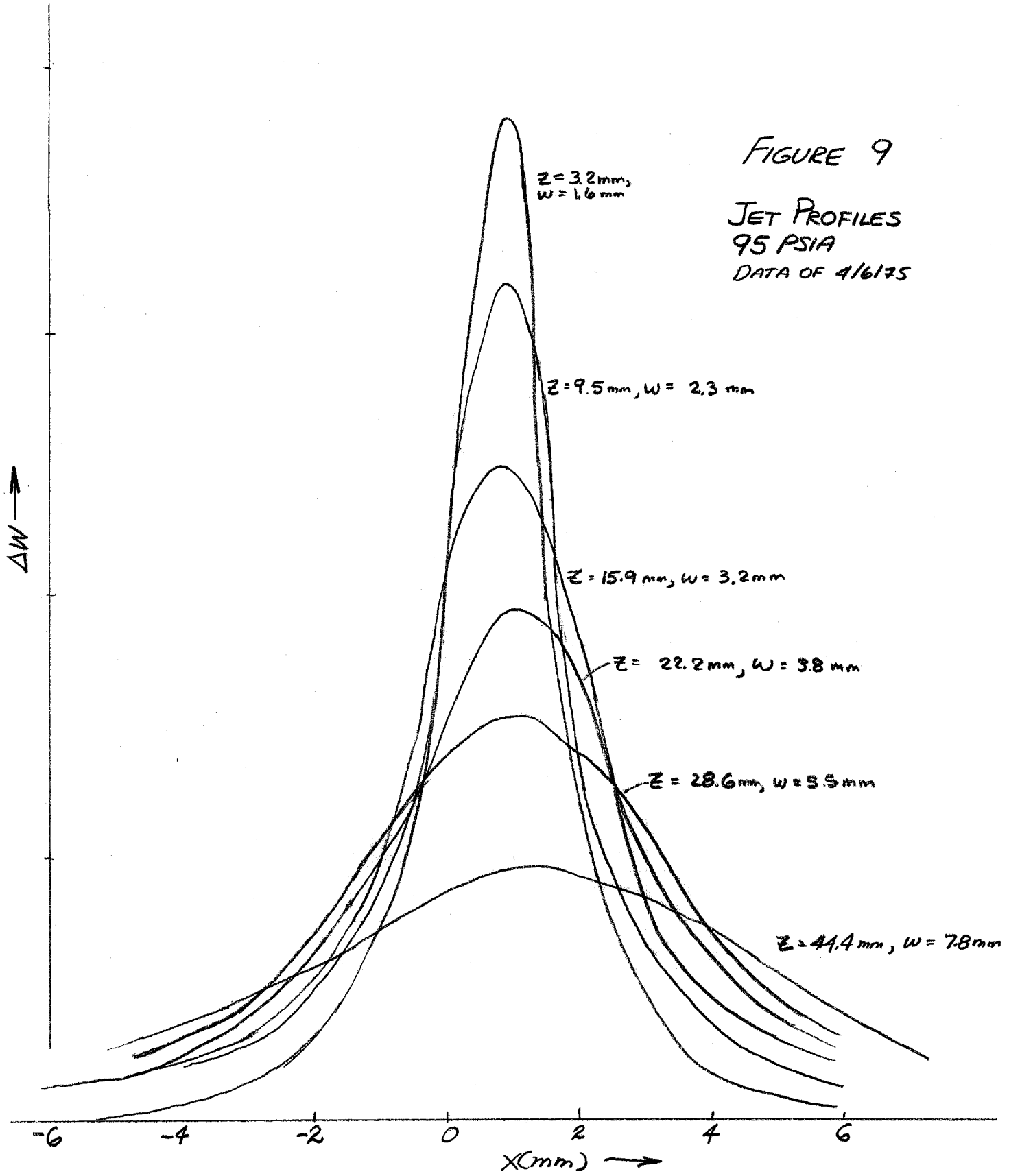
FIGURE 9
JET PROFILES
95 PSIA
DATA OF 4/6/75
z = 3.2mm, w = 1.6 mm
z = 9.5 mm, w = 2.3 mm
z = 15.9 mm, w = 3.2mm
z = 22.2mm, w = 3.8 mm
z = 28.6mm, w = 5.5 mm
z = 44.4 mm, w = 7.8mm
ΔW
-6
-4
-2
0
2
4
6
X(mm)

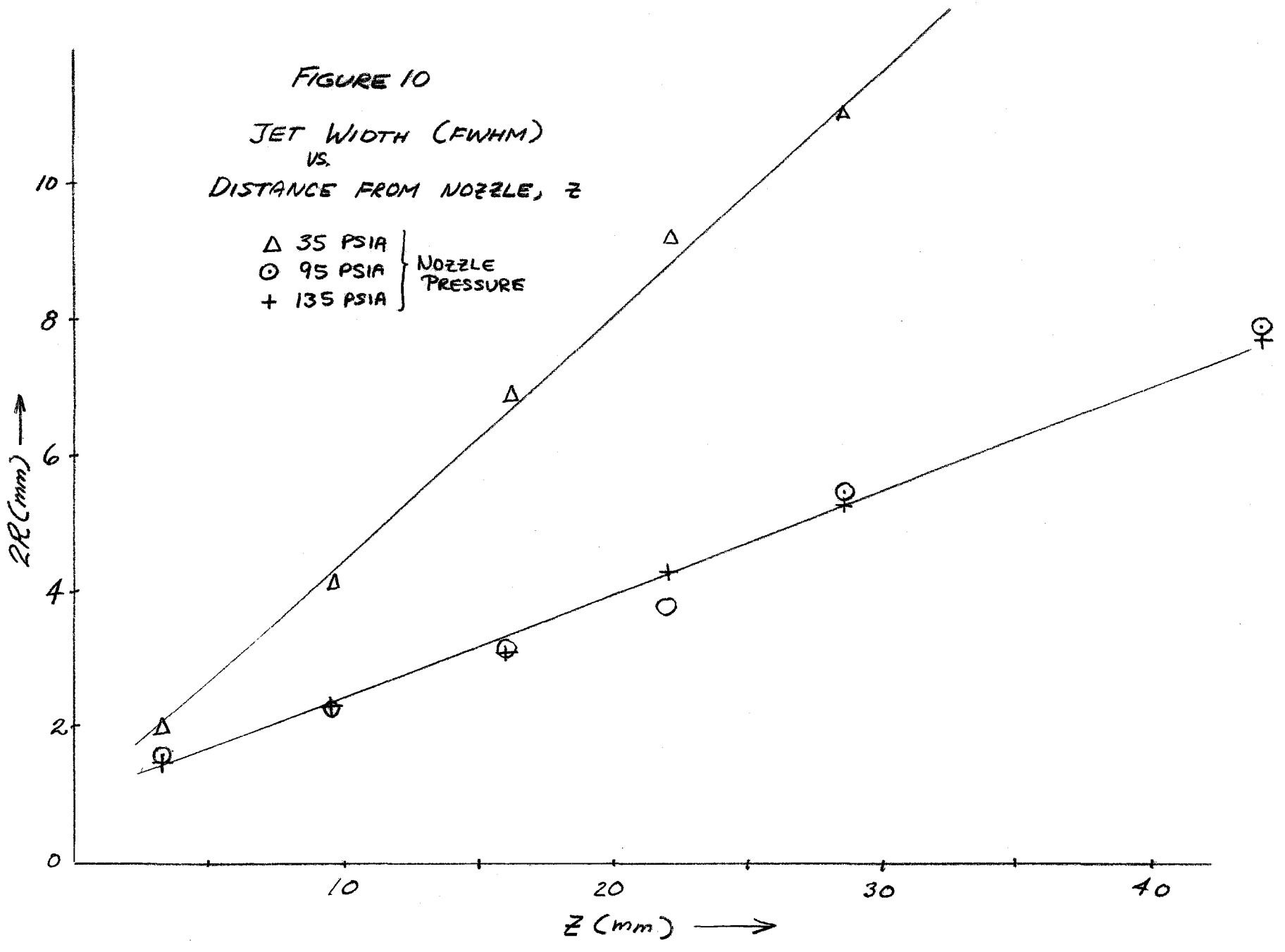
FIGURE 10
JET WIDTH (FWHM)
VS.
DISTANCE FROM NOZZLE, z
Δ 35 PSIA
⊙ 95 PSIA
+ 135 PSIA
NOZZLE PRESSURE
2R (mm) ⟶
0
2
4
6
8
10
10
20
30
40
z (mm) ⟶

7. Results

7.1 Jet Profile and Density Measurements

Figure 9 shows the profile measurement made at a nozzle pressure of 95 PSIA. The background was subtracted before the data were plotted. The sight skewing in the peaks of the profiles as the nozzle was moved away from the probe derives from the nozzle not moving exactly vertically.

The jet width (FWHM ≡ 2R) for each profile is plotted against its displacement from the tip of the nozzle. In Fig. 10, pulse width vs Z is plotted for each pressure measured. In the case of the higher pressures (95 PSIA & 135 PSIA) the jet shape is the same with an opening of about 9°. At 35 PSIA, however, the jet has opened up to 20°. Other measurements suggest that the transition to a narrow profile occurs at ~ 40 PSIA.

The density of the jet is calculated by using the peak power for given profile and the absolute density calibration of the wire. The resulting number must then be corrected by the ratio of the width of the jet divided by the probe wire length. If, for these pressures we assume a reasonable beam-nozzle distance of 25 mm, the corresponding densities are shown and compared with the flow model (see Sec. 4.1).

nozzle pressure, P_o	measured density	predicted density
"35" PSIA (2.23 atm)	$.032 \times 10^{-7}$ g/cm^3	$.049 \times 10^{-7}$ g/cm^3
"95" PSIA (6.14 atm)	$.42 \times 10^{-7}$ g/cm^3	$.59 \times 10^{-7}$ g/cm^3
"135" PSIA (8.76 atm)	$.63 \times 10^{-7}$ g/cm^3	$.84 \times 10^{-7}$ g/cm^3

The measured densities appear to be 0.7 of the predicted values; given the approximations made and the precision of the CTA calibration, this level of agreement is satisfactory.

7.2 Pressure Transients

Pressure transients of the general background H_2 gas in the chamber associated with pulsing of the jet were measured for three configurations (see Fig. 5):

a) no baffle between upper chamber and 10" ODP2,

b) baffle with 3.8 cm diameter hole

c) baffle with 6.4 cm diameter hole.

In all cases the vertical position of the nozzle could be adjusted over a 24 cm range.

The H_2 gas flow through the .004" (diameter) Los Alamos nozzle for T_o = 295°K can be calculated from eq. (7) to be

$$Q = 6.11\ P_o\ (\text{atm}) \quad \frac{\text{atm - cm}^3}{\text{sec}}$$

$$= 4.65\ P_o\ (\text{atm}) \quad \frac{\text{Torr - } \ell}{\text{sec}}$$

Q was measured by noting that this nozzle exponentially discharged (into a static vacuum) a 12.5 cm^3 volume with a time constant of 2.05 sec.

$$Q_{MEASURED} = \frac{12.5\ \text{cm}^3}{2.05\ \text{sec}} = 6.10\ \frac{\text{atm - cm}^3}{\text{sec}}$$

7.2.1 No Baffle Case

For this case we have (see Fig. 5)

$$S_{TOT} = 5650 + 390 = 6040\ \ell/\text{sec},\ V + 100\ \ell.$$

$$\tau \equiv V/S_{TOT} = 16.6\ \text{msec}$$

During this test we had a time dependent Q of the form (t_Q = 640 msec.)

$$Q = 4.65\ P_o\ (\text{atm})\ e^{-t/640}\ \text{Torr-}\ell/\text{sec.}$$

Hence for $t << t_Q$ we predict

$$P(t) = \frac{\langle Q(t) \rangle}{S_{TOT}} \left(1 - e^{-t/16.6}\right), \qquad (19)$$

where $\langle Q(t) \rangle = \frac{1}{t} \int_o^t Q(t')dt'$,

and P(t) to go through a maximum at $t_{max} = \tau\ \ln\left(\frac{2\tau_Q + \tau}{\tau}\right) =$ 72 msec, which for P_o = 1.59 atm is

$$P_{MAX} = \frac{.944 \times 4.65 \times 1.59}{6.04} \left(1 - e^{-72/16.6}\right) \times 10^{-3} = 1.14 \times 10^{-3}\ \text{Torr}$$

Figure 11 shows the IG response under these conditions for two vertical positions of the nozzle (4" from top of ODP2 and 8"). We see essentially the predicted response, but with a pressure peak of 1.5×10^{-3} t, about 32% high. We observe less than a 10% Z dependence over the 8" range. It appears then that their is no enhanced pumping by ODP2 by having the gas stream directed into its throat at this value of Q (lateral nozzle position was half way between edge of chimney top and outer wall of pump); the H_2 gas cannot be removed quickly enough from the region below the oil-vapor jet, so it diffuses backward up the pump.

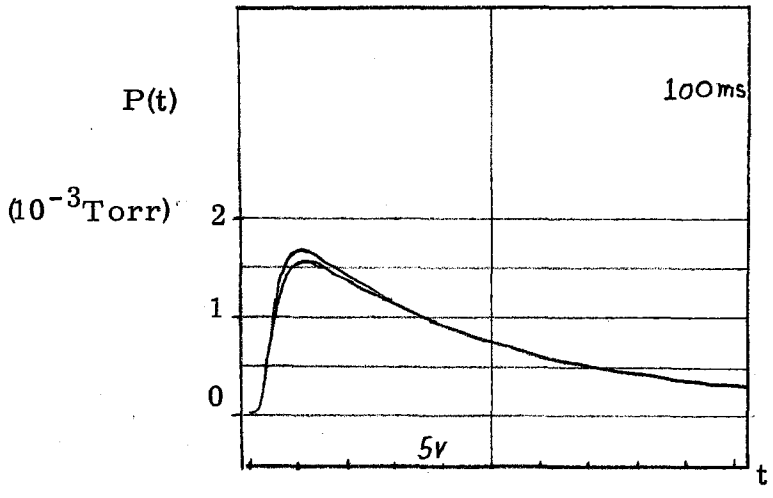

I.G. response with no baffle, P_o = 1.59 atm.

Fig. 11

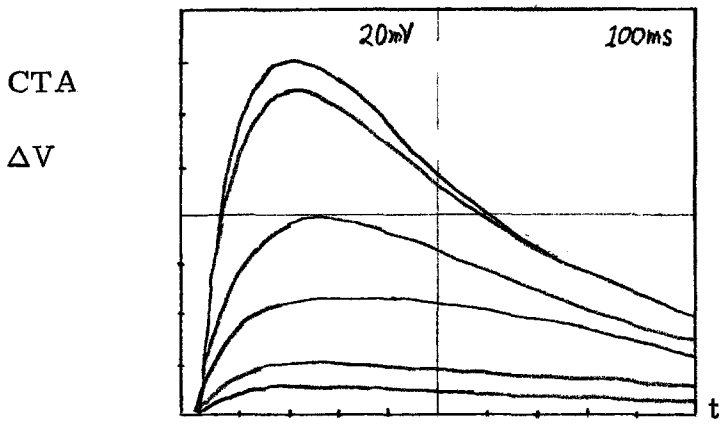

CTA response for six positions of nozzle at P_o = 4.81 atm. Z = 17, 12, 7, 4.6, 2.1, 0.8 cm.

Fig. 12

7.2.2 Baffle with 3.8 cm Aperture

In Fig. 12 we show the pressure in the upper chamber versus time for six vertical positions of the nozzle, ranging from 17 cm above the aperture to 0.8 cm above with P_o = 4.81 atm; the peak pressure drops by 15 as the nozzle approaches the hole (at the lowest position the nozzle itself must reduce the back conductance of the hole). For this P_o we have

$$Q = 22.35\ e^{-t/640}\ \text{Torr-}\ell/\text{sec.}$$

Hence the pumping parameters of the upper and lower chambers separately, i.e. if there were no connecting hole, are

$$\tau_U = \left.\frac{V}{S}\right)_U = \frac{70}{390} = 179\ \text{msec},\quad \tau_L = 5.3\ \text{msec}$$

$$\left.\frac{Q}{S}\right)_U = \frac{22.35}{390} = 57.3 \times 10^{-3} t;\quad \left.\frac{Q}{S}\right)_L = 3.95 \times 10^{-3}\ \text{Torr}$$

At the 17 cm position very little of the jet goes directly through the 3.8 cm hole, and the prediction is easily seen to be

$$S = 390 + \left(\frac{1}{5650} + \frac{1}{507}\right) = 855\ \ell/\text{sec};\quad \tau = \frac{70}{.855} = 81.9\ \text{msec}$$

$$P_U(t) = \frac{\langle Q(t) \rangle}{.855} \times 10^{-3} \left(1 - e^{-t/81.9}\right)$$

$$t_{max} \doteq 81.9\, \ell n \left(\frac{2 \times 640 + 81.9}{81.9}\right) = 230\ \text{msec}$$

We observe a peak at t = 200 msec; evaluating P_U at 200 msec gives

$$P_U(200) = \frac{19.11 \times 10^{-3}}{.855} (.913) = 20.4 \times 10^{-3}\ \text{Torr}$$

The CTA reads 17.5×10^{-3} at the peak; the agreement may be "too good" in view of the facts that at 20×10^{-3}Torr the molecular flow assumption may be questionable, and that the pressure at the head of ODP1 will be $\sim 5 \times 10^{-3}$t where it may begin to lose pumping speed.

We now proceed to estimate the fraction ϵ, of the jet gas that goes through the 3.8-cm hole when the nozzle is 4.6 cm away. From Fig. 12 we observe $P_{max} = 5.0 \times 10^{-3}$ at $t \cong 260$ msec for this position. If all of the jet gas were to pass through, then an upper limit (pertains if $P_U = 0$ for all t) of the amount which flows back is $F_a/S_L = 507/5650 = 9\%$. The simplest way to estimate ϵ is to calculate $P_U(t = 250$ ms) assuming none of the gas goes downward through the hole and compare it with the observed 5×10^{-3}t. Using the above parameters we have

$$P_U\ (t = 250\ \text{msec}) = \frac{\langle Q(250) \rangle}{390} \left(1 - e^{\frac{-250}{179}}\right) = 36 \times 10^{-3}\text{Torr}$$

Hence one estimates

$$1 - \epsilon = 5/36 = .14,\ \epsilon = .86$$

From this one can show that $P_L(t) \cong 3.4 \times 10^{-3}$Torr and decreasing with the 640 msec time constant; hence for $t > 60$ msec, $P_U > P_L$ and the molecular flow is from upper to lower through the hole.

A value for ϵ can also be obtained from the profile curves of Fig. 8; ϵ should be the fraction of the area under the curve that lies inside of $x = \pm 19$ mm at $Z = 46$ mm. Measurements at $Z = 44.4$ mm do not extend out to $x = 19$ mm, so one must resort to using the shape as determined at smaller Z to do the integration; this procedure gives $\epsilon = .92$, somewhat larger than the experimental estimate.

CTA

ΔV

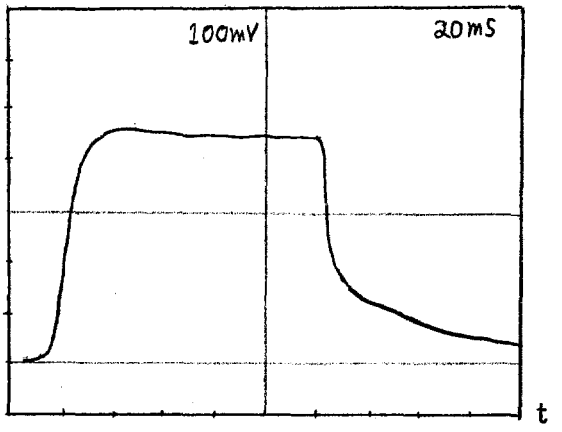

CTA response with wire 2.54 cm from nozzle at P_o = 6.14 atm. SV3 opened at t = 100 msec.

Fig. 13

7×10^{-3}Torr

CTA

ΔV

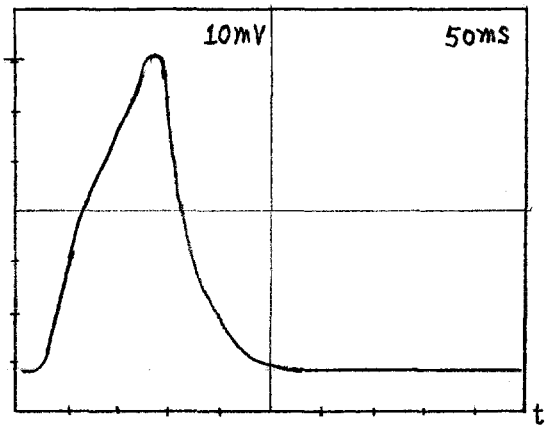

CTA response for background gas pressure for P_o = 7.6 atm. SV3 opened at t = 100 msec.

Fig. 14

IG

(10^{-3}Torr)

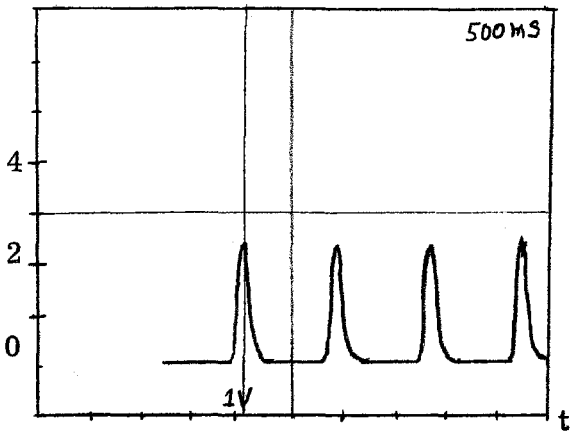

Background pressure at 1 sec rep. rate, 100 msec pulses, P_o = 5.42 atm.

Fig. 15

7.2.3 Baffle with 6.4 cm Aperture and Short Pulse

For these measurements we ran with τ_Q = 2.05 sec and terminated the pulse after 100 msec by opening SV3 (see Fig. 5). In addition, ODP1 was changed from a 4" to a 6" pump, giving an increase in S from 590 to 1200 ℓ/sec. Figure 13 displays the jet density vs t with the CTA 2.5 cm below the nozzle and P_o = 6.14 atm. Figure 14 shows the buildup of the background pressure at P_o = 7.6 atm for the same 100 msec pulse when the nozzle is 5.1 cm from the hole in the baffle. The average value during the 100 msec pulse ($\rho_{JET} = .7 \times 10^{-7}$ gm/cm^3) is 3.6×10^{-3}Torr, which is ~ 1/180 the density in the jet. Finally in Fig. 15 we show background pressure for continuous pulsing at 1-sec repetition rate with 100 msec pulses at P_o = 5.42 atm.

7.3 Comparison of LHe and RT Jet Targets

In this section, we shall compare the basic parameters of the two jets, the quantities R, ρ, Q, F, ρ/ρ_M and $\rho\ell$ as defined in Sec. 4.1 and 4.2. Since the width of the jet, 2R, is a function of the nozzle-to-beam-center distance (Z), we must adopt a specific geometry for the comparison. We take the simplest possible geometry, viz. a vertically directed jet with no material within ± 2.5 cm of the beam center; this implies a nozzle-to-beam-center distance of 2.5 cm. The data on R vs Z for the RT jet is given in Fig. 10. The LHe jet is normally run at Z = 15 mm where R has been measured by several groups[7,12] to be in the range of 6-9mm; there appears to be a dependence on T_o and P_o which may account for the spread in measurements. At Z = 2.5 cm, the measurements give R in the range 9-14 mm; for our comparison, we shall make the somewhat arbitrary but reasonable choice of R = 12 mm at Z = 2.5 cm.

To compare the two targets directly with respect to the other parameters is difficult since direct measurements of ρ and Q are not available for the LHe target. However, the good agreement between the measurements made on the RT jet and the simple model of Sec. 4 encourages one to use this model and the measured R values.

7.3.1 Comparison of Nozzles

The 0.03-cm nozzle run at T_o = 20-40°K and $P_o \sim$ 1atm clearly has a much larger divergence than does the .004" (.0102 cm) Los Alamos nozzle at T_o = 295°; the half angle for the former is 26° and for the latter 5°. (For P_o < 3 atm the Los Alamos nozzle divergence increase to ~ 10°.) In terms of R at Z = 2.5 cm, R_{He} = 12 mm, R_{LA} = 2.5 mm.

The gas flow, Q, through the nozzle depends on r, P_o, T_o and the temperature (Ti) at which you measure Q; eq.(7) gives[13]

$$Q_{LA}\ (.0102\ \text{cm},\ 295^{\circ}\text{K}) = 6.113\ P_o\ (\text{atm})\ \frac{\text{atm-cm}^3}{\text{sec}}$$

$$Q_{He40}(.15\ \text{mm},\ 40^{\circ}\text{K}) = 145\ P_o\ \frac{\text{atm-cm}^3}{\text{sec}}$$

$$Q_{He20}(.15\ \text{mm},\ 20^{\circ}\text{K}) = 205\ P_o\ \frac{\text{atm-cm}^3}{\text{sec}}$$

(to convert to $\frac{\text{Torr-}\ell}{\text{sec}}$ multiply by 0.76). Hence the LHe jet nozzle has ~ 28 times the flow for the same P_o, most of which comes from the larger area of the throat (71×10^{-3} mm^2 compared to 8.1×10^{-3} mm^2).

We compare ρ values at Z $\simeq$ 2.5 cm using eq. (5),

$$\rho_{LA} = 0.888 \times 10^{-1} \times P_o \times 10^{-7} \text{ gm/cm}^3$$

$$\rho_{He40} = 2.48 \times 10^{-1} \times P_o \times 10^{-7} \text{ gm/cm}^3$$

$$\rho_{He20} \quad 4.97 \times 10^{-1} \times P_o \times 10^{-7} \text{ gm/cm}^3,$$

the LHe jet being ~ 4 times higher for the same P_o. It follows then that the figure of merit, $F = \rho/Q$, is ~ 7 times lower for the LHe nozzle; if one uses $F' (\equiv R\rho/Q)$ then it is only 1.5 times lower.

The actual range of ρ available - or what is probably more relevant, $\rho\ell \equiv 2R\rho$ - depends on the range of P_o over which the jet will operate. The LHe target has been run in the range from 0.5 - 4 atm (nozzle freeze-up is a recurrent problem with $P_o < 1$ atm); the RT jet has been run from 2-8 atm. Hence the $\rho\ell$ ranges tested are

$$\rho\ell)_{LA} = 0.3 - 3.0 \times 10^{-8} \text{ gm/cm}^2$$

$$\rho\ell)_{He40} = 0.30 - 2.4 \times 10^{-7} \text{ gm/cm}^2$$

$$\rho\ell)_{He20} = 0.60 - 4.8 \times 10^{-7} \text{ gm/cm}^2$$

The upper value of $\rho\ell)_{LA}$ was dictated by the configuration of the vacuum system used for the test; Brolley[4] has run this nozzle at $P_o = 68$ atm (corresponding to a $\rho\ell = 3 \times 10^{-7}$ gm/cm^2) and obtained profiles similar to ours. With the LHe target, the upper limit will presumably come when the cryotrap begins to have an appreciable loss of efficiency due to the high pulsed load. In practice, the upper limit may be dictated by the main ring requirements as mentioned in Sec. 2.2.

7.3.2 Comparison of Background Gas Density

We have seen in Sec. 7.2 that the behavior of the transient in the background gas pressure during the jet pulse is predictable. Eq. (16) gives the ratio of ρ_{JET}/ρ_{BKG} as a function of time during the pulse, if $t_o >> \tau$, the ratio is essentially constant during the pulse, if $t_o << \tau$ then the ratio decreases during the pulse like $(t)^{-1}$ giving

$$\langle \rho_{JET}/\rho_{BKG} \rangle = 2 \times (\rho_{JET}/\rho_{BKG} \text{ at } t = t_o)$$

So for the test system described in Sec. 7.2.2 we obtain

$$\langle \rho_{JET}/\rho_{BKG} \rangle = 227$$

which compares to the directly measured value of 170.

For the LHe target one obtains (t_o = 250 msec, τ = 100 msec)

$$\langle \rho_{JET}/\rho_{BKG} \rangle_{40^o} = 206, \quad \langle \rho_{JET}/\rho_{BKG} \rangle_{20^o} = 291$$

A better parameter to compare may be $L \equiv \langle \rho_{JET} \times \ell/\rho_{BKG} \rangle$

$= 2R \langle \rho_{JET}/\rho_{BKG} \rangle$, which is the length of background gas having the same $\rho\ell$ as the target; this yields

$$L_{RT} = 227 \text{ cm}$$

$$L_{He40} = 494 \text{ cm}, \quad L_{He20} = 698 \text{ cm}.$$

L_{RT} is worse by ~ 2.6; this limitation is not fundamental, it is due to the fact that ODP1 is rather small.

We can summarize the comparison as follows:

a) the Los Alamos nozzle operated at 295°K has a considerably better ρ/Q than the Dubna nozzle operating at 30°K;

b) the LHe target attains a 10 x higher $\rho\ell$ than the 295° test target, but may not be able to cover the low range ($\rho\ell < 3 \times 10^{-8}$ gm/cm^2) with its present nozzle;

c) the LHe target has a 5 x wider jet at Z = 2.5 cm, giving an effective source size ~ 2.4 cm, which for some experiments is too large.

8. Summary and Conclusion

8.1 Accomplishments with the Los Alamos 0.004"-Diameter Nozzle

A test bench gas jet target using the Los Alamos de Laval was set up and run with H_2 gas at room temperature (295°K). In addition to the nozzle, the basic components of the system were: (a) a 10" oil diffusion pump, (b) a 4" oil diffusion pump, and (c) a three-solenoid system for generating a square jet pulse. With this simple system, we were able to make a prototype target that had the capabilities to:

(1) run continuously with 100-msec long pulses spaced by 1 sec;[14]

(2) give a 5 mm wide jet (FWHM) at 2.5 cm from the nozzle tip;

(3) vary $\rho\ell$ over the range 0.3 - 3 x 10^{-8} g/cm^2;

(4) yield a ratio of background gas density to jet of 1/200;

(5) transmit 86% of the directed jet gas through a 3.8 cm diameter hole 5.1 cm below the nozzle tip.

In addition, we have developed a quantitative understanding of the behavior of a target system which can serve as a basis for designing an operational target for use at CO.

8.2 Feasibility of a Gas Jet Target Operating at 295°K

We conclude from the study presented here that a gas jet target operating at room temperature is entirely feasible. From the measurements made one can infer that it is possible to design a practical target that will be compatible with the constraints imposed by C0 and which will improve on the performance of the prototype as follows:

(1) $\rho\ell$ range from 0.3 - 10 x 10^{-8} g/cm^2

(2) ρ/ρ_{BKG} = 1000

(3) at the low end of the $\rho\ell$ range the jet could run continuously with ambient pressure ~ 10^{-4}t; at the high end it would be 40 msec pulses every 330 msec.

A specific design for a target with these capabilities will be given in a companion TM.

8.3 Advantages of a Room Temperature Gas Jet Target

8.3.1 To Physics Experiments

1. Full duty cycle, 24 hr/day and 7 day/wk operation, zero startup time.
2. High reliability, expected to be operational ≥ 90% of scheduled time.
3. Smaller size of interaction region, FWHM = 5 mm.
4. Smaller target thickness available, down to.3 x 10^{-8} gm/cm^2.
5. Very little material surrounding beam; no material in ± 2.5 cm vertically and ≤ 200 g in a cylinder of diameter 12 cm around the beam.
6. Any non-corrosive gas can be used with no changes necessary.
7. Good access to the interaction region for additional detector systems, 360° in median plane and a large fraction of the upper hemisphere.
8. Nozzle easily aligned with beam.
9. If a failure occurs, target can be "fixed" in a 1-hour access.

8.3.2 To Accelerator

1. No need to turn off beam.
2. No horizontal or vertical aperture limitations (± 2.5 cm vertical).
3. No danger of He leaks into main ring or unexpected pressure bursts due to accidental sublimation of condensed gas.
4. Fits easily into existing tunnel.

8.3.3 To Internal Target Area Operations

1. No technician manpower needed for normal operation.
2. No liquid He or liquid N_2 required.
3. Essential parts replaceable in a 1-hour access.
4. Spare parts relatively cheap and easily pre-tested.
5. Little upstairs floor space required for target control system (~1/3 of one standard relay rack).

8.3.4 Disadvantages

1. Target thickness, $\rho\ell$, limited to 10×10^{-8} gm/cm^2 (H_2 gas); one could possibly go to 2×10^{-7} gm/cm^2 if the pulse length were reduced from 40 to 25 msec.
2. A partial pressure of diffusion pump oil vapor present surrounding the jet at the level of 1×10^{-8}t.

9. Acknowledgements

It is a pleasure to acknowledge Dr. J. F. Brolley of the Los Alamos Scientific Laboratory for the use of his de Laval nozzle. We are grateful to the technical staff of the Internal Target Area for general support during the course of this study. Finally, we are indebted to J. Lee-Franzini for the use of the 10" diffusion pump.

References

1. For a recent summary of this technique and the particle physics aspects, see A. C. Melissinos and S. L. Olsen, "Physics (and Technique) of Gas Jet Experiments," U. of Rochester Report (1974) (to be published in "Physics Reports").

2. For a more detailed description of the hardware, see V. Bartenev et al, "Cryopumped, Condensed Hydrogen Jet Target for the National Accelerator Laboratory," Adv. Cryogenic Eng. 18, 460 (1973).

3. See Fermilab Experiment #289 Proposal.

4. a) D. A. Gross and A. Melissinos, "Production of a High Density Hydrogen Gas Jet," U. of Rochester Report UR-875-365 (1971).
b) J. F. Brolley, "Density Profiles of a Supersonic Jet Target," IEEE Nuclear Science 20, No. 3, 475 (1973).
c) P. Franzini and J. Lee-Franzini, private communication (1975).

5. B. A. Prichard and F. Turkot, private communication (1975); see also B. A. Prichard, "Pressure Induced Beam Instabilities in the Fermilab Accelerator," to be published in IEEE Nuclear Science, June 1975. Note the ion gauge calibration given there reads too low by a factor of 15 (see Sec. 6.2).

6. L. Golovanov et al., "Evaluation of the Possibility of Cryopumping Helium Jet by Means of a Parallel Stream of Hydrogen Condensing on a 4.2°K Surface," Fermilab report TM-515 (1974), and private communication.

7. A measurement of the density distribution along the beam direction by observing recoil protons near 90° yields a ratio of ~ 300 at a distance of 4.5 cm from the jet, see K. Goulianos, "Density Profile of the Jet Target," Nov. 1974 (unpublished).

8. Recently,efforts have been made to reduce the liquid He consumption of the target through design modifications, preliminary results (private communication from S. Mukhin indicate ~ 6 ℓ/hr.
9. For a description of gas flow in a de Laval nozzle, see R. Courant and K. O. Friedrichs, Supersonic Flow and Shock Waves, P 1-28 and P 377-387, Interscience Publishers, N.Y. (1948).
10. See Handbook of Vacuum Physics (edited by A. H. Beck), Vol. 1, P 334-344, Pergamon Press, N.Y. (1966)
11. The ion gauge system used was made by Granville-Phillips Co. (Boulder, Colorado) and consisted of a Bayard-Alpert type gauge and a Series 236 (Model 02) controller. All measurements were made on the "emission multiplier" setting of 0.01, which presumably gives an emission current of 100 μA.
12. (a) D. Gross, P. Mantsch, and F. Turkot, "Measurement of the Profile of the Gas Jet Target at the Internal Target Area," Fermilab Report TM-534 (1975).
(b) Experiment 321, "Hydrogen Jet Test Report," Dec., 1974.
13. We calculate for two temperatures for the LHe target nozzle, 20°K and 40°K; the actual temperature may rise by ~ 10°K during the pulse, see Ref. 2 above.
14. Pulses as short as 20 msec can be generated with this system.